Available online at www.sciencedirect.com
SCIENCE DIRECT
International Journal of Mass Spectrometry 247 (2005) 18–27
International Journal of Mass Spectrometry
www.elsevier.com/locate/ijms

Photoionization cross sections for reaction intermediates in hydrocarbon combustion

Terrill A. Cool [a,*], Juan Wang [a], Koichi Nakajima [a], Craig A. Taatjes [b], Andrew McIlroy [b]

[a] *School of Applied and Engineering Physics, 228 Clark Hall, Cornell University, Ithaca, NY 14853, USA*
[b] *Combustion Research Facility, Sandia National Laboratories, Livermore, CA 94551, USA*

Received 31 March 2005; received in revised form 29 August 2005; accepted 29 August 2005
Available online 17 October 2005

Abstract

Previously unmeasured absolute photoionization cross sections are presented for eight common reaction intermediates found in the combustion of many simple hydrocarbons. Total photoionization cross sections recorded for 11 additional hydrocarbons are in good agreement with previous studies. The measurements are performed with photoionization mass spectrometry (PIMS), using VUV synchrotron radiation. Absolute cross sections for molecular and dissociative photoionization are determined by comparison of the photoionization efficiencies for each intermediate with that of propene, used as a calibration standard, for photon energies from 9.7 to 11.75 eV, recorded with a photon energy resolution of 50 meV(fwhm).

Keywords: Photoionization cross sections; Hydrocarbons; Photoionization mass spectrometry (PIMS); Combustion chemistry

1. Introduction

Photoionization mass spectrometry (PIMS) and dipole electron-ion (e, e + ion) coincidence spectroscopy are widely used for determinations of cross sections for parent and dissociative photoionization of molecules [1]. Near-threshold PIMS measurements of *relative* photoionization cross sections yield adiabatic ionization energies, photofragment appearance thresholds, proton affinities, ionic heats of formation and related thermochemical properties [2].

Absolute photoionization cross sections of good accuracy for numerous atoms and simple molecules, measured with these well-developed techniques, find applications in atmospheric and astrophysical photochemistry and modeling of fundamental photo-physical processes [1,3,4]. Although measurements of near-threshold relative cross sections (photoionization efficiency (PIE) curves) are available for many molecules [3–5], reliable measurements of absolute cross sections are less common. Cross sections obtained with the equivalent dipole electron-ion coincidence (e, e + ion) method are typically measured with an energy resolution ΔE (fwhm) ≈0.5–1.0 eV, limited by the thermal spread of the electron beam [1,6]. The much higher working resolution, $E/\Delta E$ (fwhm) ≈400–2000, available with monochromated synchrotron radiation [7–10] makes PIMS the method of choice for measurements of ionization energies, appearance potentials, and near-threshold cross sections for parent ion and fragment ion formation.

The use of PIMS for quantitative studies of flame chemistry [11–14] has recently generated renewed interest in measurements of absolute photoionization cross sections to supplement relative photoionization efficiencies traditionally used for determinations of ionization energies and thermochemical properties. Kinetic models of hydrocarbon combustion may incorporate hundreds of chemical reactions involving several dozen key reaction intermediates for which photoionization cross sections are required. Reliable measurements of absolute cross sections for near-threshold total positive ion production using the single ionization cell [15,16] and more popular double-ionization chamber [1,17–19] methods are available for several simple hydrocarbons of interest in combustion chemistry [3,20–27]. For many hydrocarbons, however, the appearance energies for dissociative ionization are within 1–2 eV of the adiabatic ionization energy of the parent molecule and *mass-resolved* ion detection is required to distinguish the partial contributions to the total

* Corresponding author. Tel.: +1 607 255 4191; fax: +1 607 255 7658.
E-mail address: tac13@cornell.edu (T.A. Cool).

1387-3806/$ – see front matter © 2005 Elsevier B.V. All rights reserved.
doi:10.1016/j.ijms.2005.08.018

photoionization cross section made by dissociative ionization channels. Indeed, in PIMS studies of flame chemistry, ion fragments of a given mass-to-charge (m/z) ratio may interfere with the detection of parent ions with the same m/z value. Successful strategies for quantitative measurements of flame species composition often require partial photoionization cross sections for many such dissociative channels [12].

Studies of hydrocarbon combustion with synchrotron PIMS have been performed with our apparatus with photon energy spreads ranging from 25 to 60 meV [11–14]. Quantitative determinations of flame species concentrations require absolute photoionization cross sections of comparable resolution, preferably measured under experimental conditions corresponding to those used in the flame chemistry studies. In this paper, we present previously unmeasured absolute photoionization cross sections for eight common hydrocarbon combustion intermediates for photon energies from 9 to 11.75 eV, recorded at an energy resolution of 50 meV (fwhm). The photoionization cross sections presented here contribute to a growing comprehensive database critically needed for PIMS studies of hydrocarbon flame chemistry.[1]

2. Experimental

2.1. Apparatus

A molecular beam time-of-flight photoionization mass spectrometer is used for our cross section measurements. It is coupled to a 3 m off-plane Eagle monochromator, used to disperse synchrotron radiation from a 10 cm-period undulator at the Chemical Dynamics Beamline [28] of the Advanced Light Source (ALS) of the Lawrence Berkeley National Laboratory. Higher order diffraction and high-energy undulator harmonics are suppressed by passing the undulator beam through a gas filter containing argon [29].

The apparatus consists of a stainless steel gas reservoir chamber ("flame chamber") [11,12] containing a binary mixture of the "target" molecule and a "standard" species (propene) of known photoionization cross section, a two-stage differentially pumped molecular beam sampling system, and a time-of-flight mass spectrometer (TOFMS).

A nominal mixture of 0.5% each of propene and a given target molecule in 99% argon at a reservoir pressure of 9 Torr is expanded to a pressure of about 10^{-5} Torr through a 0.2 mm diameter orifice in a quartz sampling cone. A nickel skimmer with its 2 mm diameter aperture, located 23 mm downstream from the sampling cone orifice, forms a molecular beam that passes into the main test chamber and between the repeller and extractor plates of a conventional linear (Wiley-McLaren [30]) TOFMS.

The output beam from the monochromator enters the main test chamber through a differentially pumped capillary aperture, designed to provide a pressure ratio of 200 between the test chamber and the monochromator exit slit. The photon beam intersects the molecular beam at right angles at a position midway between the repeller and extractor plates of the TOFMS. Pulse gating of the repeller plate voltage propels photo-ions along a 1.3 m flight tube to a microchannel plate (MCP) detector (Burle, APD). A multiscaler (FAST Comtec P7886) records TOFMS mass spectra in 15,008 channels of 2 ns width.

The TOFMS mass resolution is typically $m/\Delta m = 400$. The monochromator, with a 600 lines/mm tungsten grating, delivers photon fluxes of about 3×10^{13} photons/s with an energy spread $\Delta E = 40$ meV (fwhm) when operated with a 400 μm exit slit in the 9–12 eV photon energy range. A silicon photodiode (International Radiation Detectors, Inc. SXUV-100) records the variation in photon flux with photon energy. The quantum efficiency (electron/photon) of the photodiode was measured over the range of photon energies from 8 to 15 eV at the National Institute of Standards and Technology.

The photon energies are calibrated by recording mass spectra for O_2^+ photo-ions for energies between 12 and 13 eV, an interval that includes several narrow autoionized members of the H and H′ vibrational progressions [31].

Binary mixtures of nominally 10 Torr propene with 10 Torr of a given target are prepared in a 3.8 l stainless steel sample cylinder, with Teflon-coated inner surface, to which an additional 2300 Torr of argon is added. The combined gases are allowed to mix for at least 8 h and then are introduced to the stainless steel reservoir chamber at a steady flow rate of 0.1 slm (standard liters per minute) along with a second flow of argon at 0.15 slm. The quartz-sampling cone is located in a sidewall of the chamber. The chamber pressure is kept constant at 9 Torr with a servo-controlled throttle valve on the chamber exhaust. This arrangement enables run times of about 1 h, during which the ratio of target ion signal to propene ion signal is recorded over the 9.7–11.75 eV photon energy range for which the absolute cross section for molecular photoionization of propene has been accurately measured by Person and Nicole [22,24]. Although the upper limit on photon energy for the present work is set by the 15.76 eV ionization potential of argon, rather than the 11.75 eV lithium fluoride cutoff for the Person and Nicole studies, we have confined the present measurements to the 9.7–11.75 eV photon energy range, except as noted in Section 3 for cyclopentene, *cis*-2-pentene, *trans*-2-pentene, 1,3-butadiene, benzene, diethyl ether, and vinylacetylene below 9.7 eV and formic acid and acetylene above 11.75 eV.

The sources of the chemicals used in these studies are as follows: propene 99+% (Aldrich), propyne 98% (Aldrich), methanol, 99+% (Aldrich), vinylacetylene 99.9% (Organic Technologies), diethyl ether 99+% (Aldrich), benzene 99+% (Aldrich), ethylene CP grade (Air Products), 1,3-butadiene CP grade (Matheson), acetylene (0.9% in 99.1% nitrogen) (Matheson), formic acid 95–97% (Aldrich), *cis*-2-pentene 98% (Aldrich), *trans*-2-pentene 99% (Aldrich), cyclohexane 99% (Aldrich), cyclopentene 96% (Aldrich), ethanol 99.5% (Aldrich), dimethyl ether 99+% (Aldrich), acetone 99.5%

[1] A repository, for photoionization cross section data has been established within the Collaboratory for Multi-scale Chemical Sciences (CMCS) at the Sandia National Laboratories: http://cmcs.org/technical.php.

(Aldrich), 1-propanol 99.5% (Aldrich), 2-propanol 99.5% (Aldrich). Diacetylene was prepared through the reaction of 1,4-dichlorobut-2-yne with potassium hydroxide according to the procedure of Armitage et al. [32].

2.2. Measurement procedure

Person and Nicole [20–24] have carefully measured total photoionization cross sections for several hydrocarbons using the dual-beam single ion chamber technique [15]. The response of their apparatus was calibrated using measured photo-ion signals for nitric oxide with the accurate photoionization cross section measurements of Watanabe et al. [16], which have been widely used as a calibration standard [26,33,34] and are in good agreement with more recent measurements [35]. Acetone was used as a secondary calibration standard for the measurement of photoionization cross sections for other molecules [15]. The dual-beam single ion chamber method used by Person and Nicole differs from the more widely used double ion chamber approach favored for more recent photoionization cross section measurements [7–10,36,37]. Both techniques give the total photoabsorption cross section and the total photo-ion yield. In the dual-beam single ion chamber method, the total photoabsorption cross section is measured separately with split-beam detection of both the incident light intensity and the intensity of light transmitted by an ionization cell. In the double ion chamber approach [17–19], the light beam passes successively through two identical sections of an ion chamber. The ion currents measured with ion collector plates in each section are used to simultaneously record both the total absorption cross section and the efficiency of total photo-ion production. Both methods require that the ion detection efficiency of the apparatus be calibrated using a gas (e.g., a rare gas or nitric oxide) with known photoabsorption and photoionization cross sections.

Our procedure is to use the total photoionization cross sections measured by Person and Nicole for eight hydrocarbons (acetylene, ethylene, methanol, propene, propyne, acetaldehyde, ethanol, and acetone) [21–24], supplemented with the double-ion chamber measurements for benzene of Rennie et al. [26], to calibrate the response of our instrument for photoionization cross section measurements of other target molecules. The calibrated response of our molecular beam TOFMS system accounts for mass discrimination effects that deplete the concentrations of beam components of light mass compared with those of heavier components [38,39]. This calibration enables the ion signal for a target molecule with a given m/z value to be directly compared to the ion signal of propene with $m/z = 42$ for photon energies from 9.7 to 11.75 eV.

The ratio of target ion signal to propene ion signal is given by the relationship:

$$\frac{S_T}{S_P} = \left[\frac{P_T}{P_P}\right]\left[\frac{\sigma_T(E)}{\sigma_P(E)}\right]\left[\frac{R_T}{R_P}\right] \quad (1)$$

Here P_T/P_P is the ratio of target to propene partial pressures in the binary gas mixture, $\sigma_T(E)/\sigma_P(E)$ is the ratio of target to propene photoionization cross sections at the photon energy E, and R_T, and R_P are mass-dependent response factors that account for differing sampling and detection efficiencies for the target and propene ions.

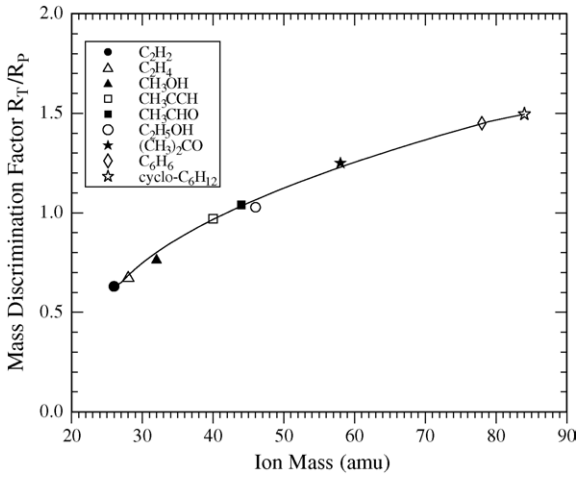

Fig. 1. According to Eq. (1), the ratio of recorded ion signals for a given target molecule to that of propene, S_T/S_P, is proportional to the ratio of photoionization cross sections, $\sigma_T(E)/\sigma_P(E)$, multiplied by the mass discrimination factor, R_T/R_P. The symbols are the mass discrimination factors given by Eq. (1) for eight target molecules for which the cross section ratio, $\sigma_T(E)/\sigma_P(E)$, is known. The solid curve is a fit to the 8 measured mass discrimination factors used to obtain photoionization cross sections for 11 other molecules for which ion signal ratios, S_T/S_P, are recorded.

In this paper, "ion signal" refers to the ion count at a given mass/charge m/z ratio, obtained by integration of the accumulated ion counts per channel over 25–40 multiscaler channels (50–80 ns) centered about the mass peak, from which the baseline contribution, obtained from the signal between peaks, is subtracted. This permits integration over the entire temporal profile of each mass peak, while avoiding overlapping contributions from adjacent mass peaks.

The ratios R_T/R_P (mass discrimination factors) [40] needed to bring our measurements of ion signal ratios [cf. Eq. (1)] into agreement with the ratios of known [21–24,26] ionization cross sections $\sigma_T(E)/\sigma_P(E)$ are displayed with symbols in Fig. 1. The solid curve of Fig. 1 is a fit to these ratios that we use to obtain mass discrimination factors, R_T/R_P, for cross section measurements of other molecules.

The comparisons of $\sigma_T(E)$ obtained from Eq. (1), using the R_T/R_P values indicated with symbols in Fig. 1, with previous absolute cross section measurements for methanol, ethanol, acetone, and benzene presented in Figs. 2–5, illustrate this procedure. Similar comparisons for acetylene, ethylene, and propyne are available as supplementary material to this paper.

Some target molecules (acetone, *cis*-2-pentene, *trans*-2-pentene, 1-propanol, cyclohexane) yield $C_3H_6^+$ fragment ions in the energy range of these studies. In these cases, supplemental measurements of the yield of fragment ions in the absence of admixed propene were performed. These measurements enabled the contributions to the $C_3H_6^+$ ($m/z = 42$) and $^{13}C_3H_6^+$ ($m/z = 43$) isotopomer signals owing to target ion fragmentation to be quantitatively distinguished from the corresponding ion signals from propene.

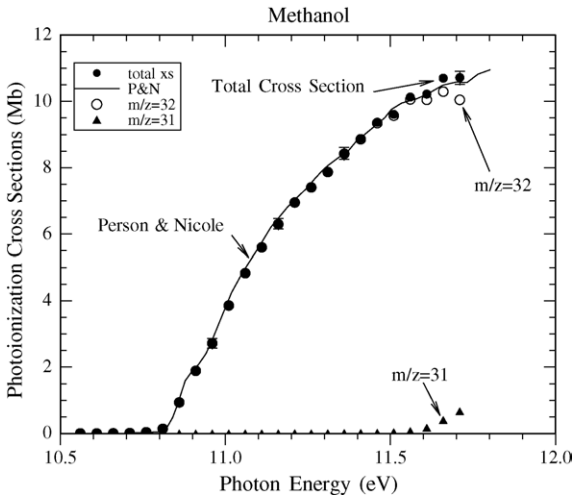

Fig. 2. A comparison of the total photoionization cross section for methanol with the previous measurements of Person and Nicole [23,24]. The comparison gives the "best fit" value $R_T/R_P = 0.77$ for methanol plotted in Fig. 1. The photon energies given by Person and Nicole have been increased by 20 meV in this comparison. The error bars shown with representative data points are the ±1 standard deviations for three separately prepared sample mixtures. 1 Mb = 10^{-18} cm^2.

2.2.1. Methanol, ethanol, acetone

Because the measurements of Person and Nicole [21–24] are not mass-resolved, the contributions of photofragment ions are included in the total photoionization cross sections they have reported. For methanol, only a small contribution from CH_3O^+ ($m/z = 31$) fragment ions is present above 11.6 eV (Fig. 2), but more extensive fragmentation is observed for ethanol and acetone, as illustrated in Figs. 3 and 4. For ethanol, the fragment ions $C_2H_5O^+$ ($m/z = 45$) and CH_3O^+ contribute substantially [5,41] to the total photoionization cross section measured previously by Person and Nicole [23,24].

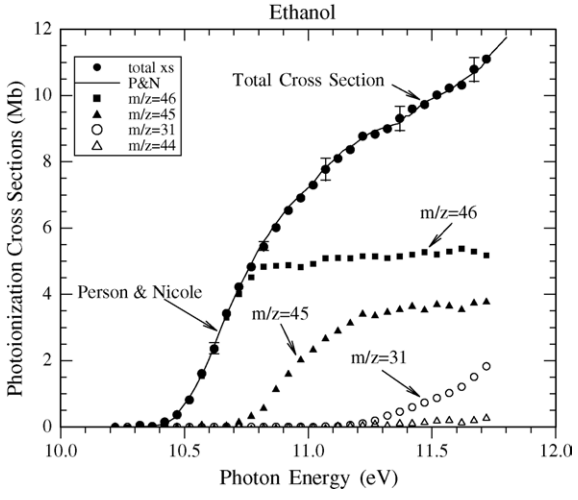

Fig. 3. A comparison of the total photoionization cross section for ethanol with the previous measurements of Person and Nicole [23,24]. The comparison gives the "best fit" value $R_T/R_P = 1.028$ for ethanol plotted in Fig. 1. The photon energies given by Person and Nicole have been increased by 20 meV in this comparison. The error bars give ±1 standard deviations for two separately prepared samples.

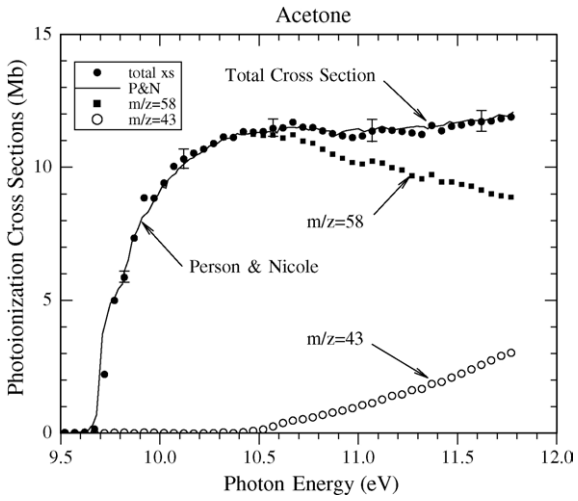

Fig. 4. A comparison of the total photoionization cross section for acetone with the previous measurements of Person and Nicole [24]. The comparison gives the "best fit" value $R_T/R_P = 1.25$ for acetone plotted in Fig. 1. The error bars give ±1 standard deviations for three separately prepared samples.

The appearance potential for CH_3CO^+ fragment ions at $m/z = 43$ from acetone is approximately 10.4 eV [5]. Cross sections for the parent $(CH_3)_2CO^+$ ($m/z = 58$) and fragment CH_3CO^+ ions are displayed in Fig. 4 along with their sum and the total photoionization cross section for acetone (solid curve) reported by Person and Nicole [24]. The contribution of ^{13}C isotopomers of $C_3H_6^+$ is subtracted from the $m/z = 43$ ion signal to determine the CH_3CO^+ fragment ion cross section. Supplemental studies of the fragmentation of acetone in the absence of admixed propene revealed $C_2H_2O^+$ fragment ions at $m/z = 42$ with an appearance energy near 10.5 eV. The fragment ion signal at $m/z = 42$ was negligible, however, being less than 0.7% of the $m/z = 58$ parent ion signal for photon energies below 11.8 eV.

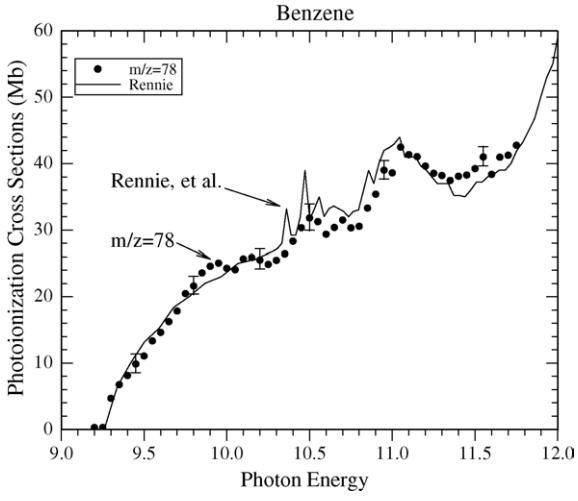

Fig. 5. A comparison of the parent ion photoionization cross section for benzene with the previous measurements of Rennie et al. [26]. The comparison gives the "best fit" value $R_T/R_P = 1.45$ for benzene plotted in Fig. 1. The photon energies of Rennie et al. have been increased by 20 meV in this comparison. The error bars give ±1 standard deviations for two separately prepared samples.

2.2.2. Benzene

For benzene, we have chosen to normalize our measurements of $\sigma(E)$ (solid circles) with the measurements of Rennie et. al. [26] (solid curve) shown in Fig. 5, performed using synchrotron radiation, a 5-m normal incidence monochromator, and a double ion chamber [7]. The photoionization efficiency (PIE) was normalized to that of nitric oxide reported by Watanabe et al. [16]. The cross sections of Rennie et al. are consistently higher than those reported by Person [20], but in better agreement with values derived from the absorption measurements of Person and Nicole [42] in a later study. The vibrational structure evident in the higher resolution measurements of Rennie et al. is not resolved in our data. This structure belongs to vibronic states of the $3e_{2g} \rightarrow 4p$ and $3e_{2g} \rightarrow 4f$ autoionizing Rydberg transitions converging onto the A^2E_{2g} ionization threshold [26]. Our benzene cross sections of Fig. 5 have been extended to include the region from threshold (9.24 eV) to 9.8 eV by using the measured ion signal for $m/z = 78$, corrected for the changes in photon flux with photon energy recorded with the calibrated photodiode.

3. Results

Eq. (1) used with the response factor ratios (fitted curve) of Fig. 1 yields absolute cross sections for binary mixtures of a given target molecule and propene. In this section, we present absolute cross sections for 1-propanol, 2-propanol, vinylacetylene, diacetylene, 1,3-butadiene, dimethyl ether, diethyl ether, *cis*-2-pentene, *trans*-2-pentene, cyclopentene, cyclohexane, and formic acid.

Because the target ion signal, corrected for changes in photon flux with photon energy with the NIST-calibrated photodiode, is directly proportional to the target ion photoionization cross section, it was possible to extrapolate the cross section measurements for cyclopentene, *cis*-2-pentene, *trans*-2-pentene, 1,3-butadiene, benzene, diethyl ether, and vinylacetylene from 9.8 eV to their ionization thresholds [5] at 9.01, 9.01, 9.04, 9.07, 9.24, 9.51, and 9.58 eV, respectively. The flux-corrected ion signals for formic acid and acetylene were also used to extend cross section measurements to 12.41 and 13.5 eV (see supplementary data), respectively. The error limits shown with the data for a few representative photon energies are the ±1 standard deviations for two to four separately prepared target/propene mixtures.

3.1. 1-Propanol and 2-propanol

Figs. 6 and 7 display the extensive fragmentation observed for 1-propanol and 2-propanol for photon energies less than 1 eV above the adiabatic ionization energy of the parent molecules. For 1-propanol, the parent ion $C_3H_7OH^+$ ($m/z = 60$) is accompanied by the major fragment ions $C_3H_6^+$ ($m/z = 42$), $C_3H_7O^+$ ($m/z = 59$) and CH_3O^+ ($m/z = 31$) with appearance energies below 11.75 eV [5,41]. Minor fragments $C_2H_5O^+$ ($m/z = 45$) and $C_3H_7^+$ ($m/z = 43$) also appear below 11.75 eV [5,41]. Measurement of the partial cross sections for the $C_3H_6^+$ and $C_3H_7^+$ dissociative channels required supplemental observations of $C_3H_6^+$ and $C_3H_7^+$ fragment ions from 1-propanol in the absence of admixed propene. In the case of 2-propanol, the total photoionization cross section is almost entirely attributable to the fragment ions $C_2H_5O^+$ ($m/z = 45$) and $C_2H_4O^+$ ($m/z = 44$) with very little $C_3H_7OH^+$ ($m/z = 60$) parent ion formation. Minor fragments $C_3H_7O^+$ ($m/z = 59$) and $C_3H_7^+$ ($m/z = 43$) are also observed below 11.75 eV [5,41]. The contribution of the ^{13}C isotopomers of $C_3H_6^+$ at $m/z = 43$ is subtracted to obtain the $C_3H_7^+$ ion signals for 1- and 2-propanol. Ionization above the second ionization potentials, 11.36 and 11.30 eV for 1-propanol and 2-propanol, respectively [43], is indicated by the increases in total ionization cross sections above 11.3 eV.

The total photoionization cross sections for 1- and 2-propanol are in reasonable agreement with the previous measurements of Koizumi and co-workers, with an estimated accuracy of 20–30%, obtained with synchrotron photoionization and a double-ionization cell [44,45]. Our absolute cross section measurements are also in good qualitative agreement with the relative photo-ion yields reported by Refaey and Chupka in their

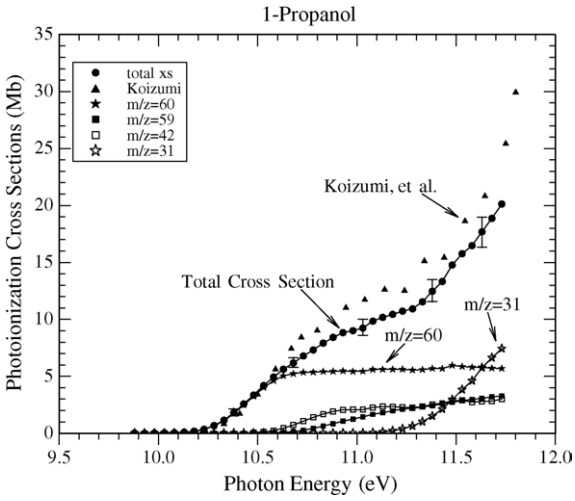

Fig. 6. Molecular and dissociative photoionization cross sections for 1-propanol. The total photoionization cross section is compared with the previous measurements of Koizumi et al. [45,46].

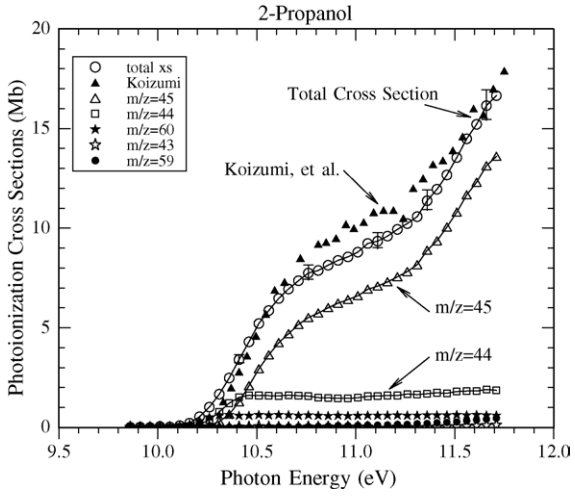

Fig. 7. Molecular and dissociative photoionization cross sections for 2-propanol. The total photoionization cross section is compared with the previous measurements of Koizumi et al. [45,46].

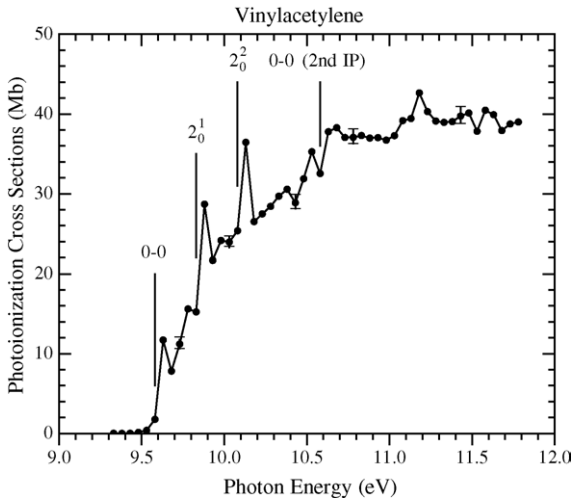

Fig. 8. Absolute cross section for the photoionization of vinylacetylene. The first and second ionization potentials and the expected energies of the $v_2' = 1, 2$ members of a progression in the C≡C stretch of the cation are indicated (see text).

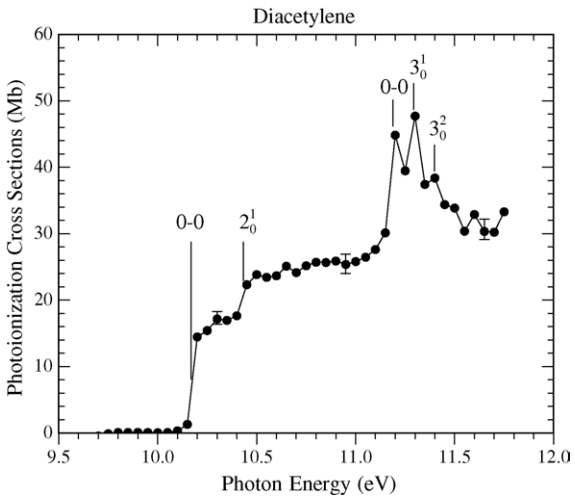

Fig. 9. Absolute cross section for the photoionization of diacetylene. The adiabatic ionization threshold at 10.17 eV and a well-defined step for direct ionization to the $v_2' = 1$ vibrational level of the cation at 10.43 eV are indicated. An origin band at 11.2 eV with partially resolved vibronic structure may belong to an autoionizing Rydberg state converging on the second ionization potential at 12.63 eV (see text).

extensive study of molecular and dissociative photoionization of methanol, ethanol, 1-propanol and 2-propanol [41].

3.2. Vinylacetylene

Fig. 8 presents the absolute photoionization cross section for vinylacetylene for photon energies ranging from 9.33 to 11.78 eV. The ratios of ion signals at $m/z = 52$ and $m/z = 42$ recorded from 9.8 to 11.78 eV are used with Eq. (1) to calibrate the photoionization efficiency for vinylacetylene against that of propene. The PIE for vinylacetylene is extended to the 9.33–9.8 eV region by using the measured ion signal for $m/z = 52$, corrected for the changes in photon flux with photon energy recorded with the calibrated photodiode.

Although the photoelectron spectrum of vinylacetylene has been recorded [46,47] over the range of photon energies of Fig. 8, no other photoionization efficiency measurements for vinylacetylene have been published. Photoelectron spectroscopy places the adiabatic ionization energy at 9.58 eV, the second ionization potential at 10.58 eV, and the frequency of the C≡C symmetric stretch of the ground state of the cation at $\upsilon_2 = 2020\ \mathrm{cm}^{-1}$ [46,47]. The first and second ionization potentials and the expected energies of the $v_2' = 1, 2$ members of a progression in the C≡C stretch are indicated by the vertical lines in Fig. 8.

The structure seen between 9.58 and 10.33 eV, with prominent broad peaks at 9.63, 9.88, and 10.13 eV, is quite reproducible with good signal-to-noise. This discrete structure suggests poorly resolved vibrational autoionization resonances, strongly broadened by predissociation, for Rydberg series converging to the $v_2' = 1, 2,$ and 3 states of the cation.

3.3. Diacetylene

Both absorption and photoelectron spectroscopy have been used to study the spectrum of diacetylene in the region between the first (10.17 eV) and second (12.62 eV) ionization potentials [5,48]. The vacuum ultraviolet absorption spectrum of diacetylene was first recorded by Price and Walsh [49], and later by Smith [48]. No previous studies of photoionization efficiency have been undertaken.

The cross section data of Fig. 9 show the adiabatic ionization threshold at 10.17 eV and the origin band of an autoionizing electronic state at 11.2 eV. The step at 10.43 eV arises from direct ionization to the υ_2 C≡C ($2177\ \mathrm{cm}^{-1}$) [50] symmetric stretch of the $C_4H_2^+$ ground state. The origin band at 11.2 eV ($90{,}330\ \mathrm{cm}^{-1}$) is accompanied by the first two members of a progression with a vibrational spacing of 0.1 eV ($807\ \mathrm{cm}^{-1}$). This spacing matches the frequency of the υ_3 C–C symmetric vibration of the $A^2\Pi_u$ state (second ionization potential) of the ion [50,51], which suggests that these bands are vibronic components of an autoionizing member of a Rydberg series leading to the $A^2\Pi_u$ state at 12.63 eV. Indeed, Smith observed a weak, strongly predissociated, absorption with no observable vibrational structure at $91{,}120\ \mathrm{cm}^{-1}$, in the vicinity of the $v_3' = 1$ peak at 11.3 eV ($91{,}140\ \mathrm{cm}^{-1}$) displayed in Fig. 9, which he assigned to the $n = 4$ member of a Rydberg series converging onto the $A^2\Pi_u$ state [48].

3.4. 1,3-Butadiene

The cross section for parent ionization of 1,3-butadiene shown in Fig. 10 is qualitatively similar to the photoionization efficiency curve recorded by Parr and Elder [52]. The parent ion cross section reaches a short plateau at 9.8 eV, rises further and then decreases rapidly beyond 11.4 eV, the appearance energy for $C_3H_3^+$ ($m/z = 39$) fragment ions. $C_4H_5^+$ fragment ions, recorded by Parr and Elder with appearance energy of 11.56 eV, were not observed at the detection limit of the present experiments. The total photoionization cross section (open circles in Fig. 10) is nearly constant between 11.4 and 11.75 eV;

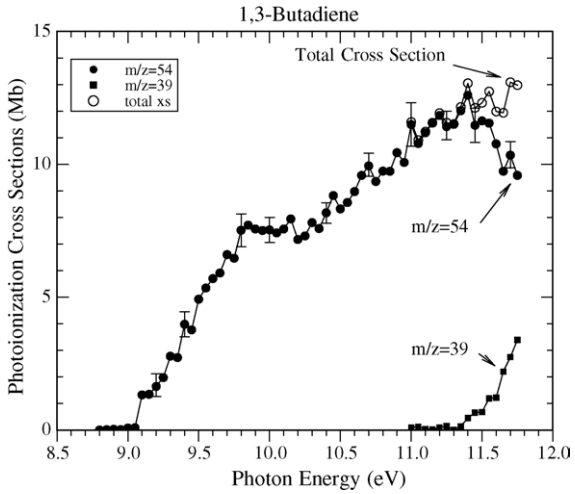

Fig. 10. Parent ion $C_4H_6^+$ ($m/z = 54$) and $C_3H_3^+$ ($m/z = 39$) fragment ion photoionization cross sections for 1,3-butadiene.

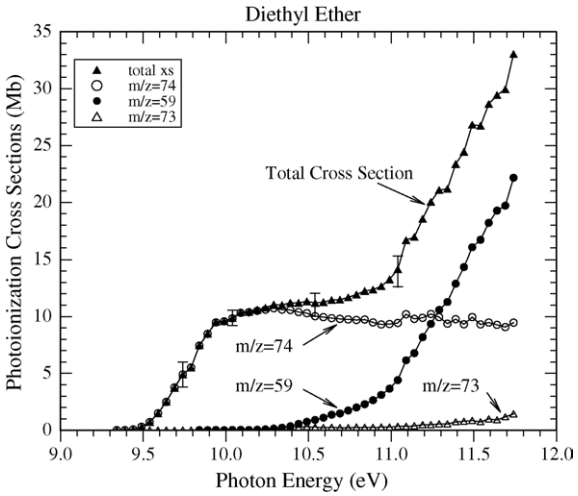

Fig. 12. Molecular and dissociative photoionization cross sections for diethyl ether.

the decrease in the parent ion cross section is balanced by the increasing partial cross section for $C_3H_3^+$, indicative of the competition between these two ionization channels.

3.5. Dimethyl ether and diethyl ether

Absolute cross sections for the photoionization of dimethyl ether and diethyl ether are presented in Figs. 11 and 12. These measurements are in good qualitative agreement with the relative photo-ion yields for molecular and dissociative photoionization of dimethyl and diethyl ether carefully recorded by Botter et al. [53]. Absolute total photoionization cross sections for dimethyl ether reported by Koizumi et al. [44,45] are in reasonable agreement with the present measurements as shown in Fig. 11.

The parent ion cross section for dimethyl ether of Fig. 11 rises smoothly from threshold at 10.03 eV [5], reaches a maximum of 10.4 Mb at the 11.0 eV [5,53,54] appearance energy for $C_2H_5O^+$ ($m/z = 45$) fragment ions, and then slowly decreases in competition with the fragmentation channel to the 11.75 eV limit of the present measurements. The total photoionization cross section rises smoothly from threshold to beyond the second ionization potential at 11.65 eV [43].

The parent ion cross section for diethyl ether ($m/z = 74$) shown in Fig. 12 rises smoothly from threshold at 9.51 eV [5], reaches a maximum of 10.7 Mb near the 10.33 eV [53] appearance energy for $C_3H_7O^+$ ($m/z = 59$) ions, and then decreases slightly over the 10.3–11.75 eV range. A second dissociative ionization channel forming $C_4H_9O^+$ ($m/z = 73$) fragment ions opens at 10.22 eV [53], but makes a much smaller contribution to the total photoionization cross section. The $C_3H_7O^+$ fragment ion and total ionization cross sections increase rapidly for photon energies exceeding the second ionization potential at 11.03 eV [43].

3.6. cis-2-Pentene, trans-2-pentene, and cyclopentene

The cross sections for *cis*- and *trans*-2-pentene shown in Figs. 13 and 14 are very similar; both rise from adiabatic

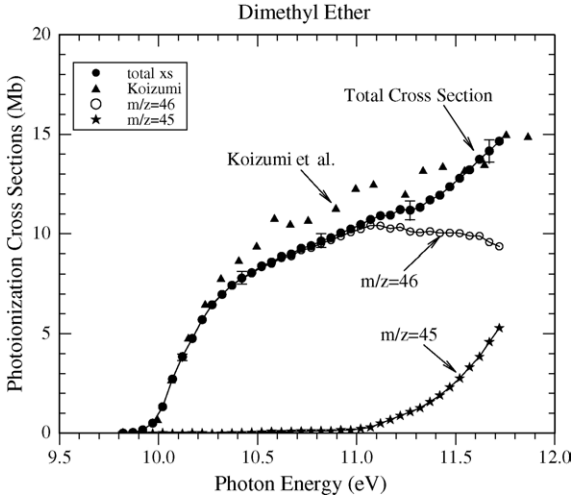

Fig. 11. Molecular and dissociative photoionization cross sections for dimethyl ether. The total photoionization cross section is compared with the previous measurements of Koizumi et al. [45,46].

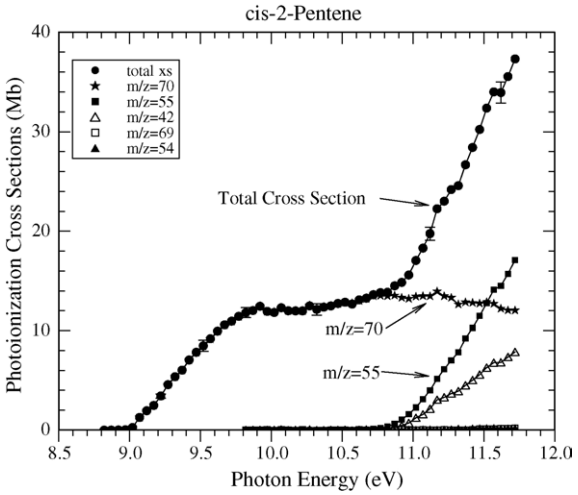

Fig. 13. Parent ion $C_5H_{10}^+$ ($m/z = 70$) and $C_4H_7^+$ ($m/z = 55$) fragment ion photoionization cross sections for *cis*-2-pentene.

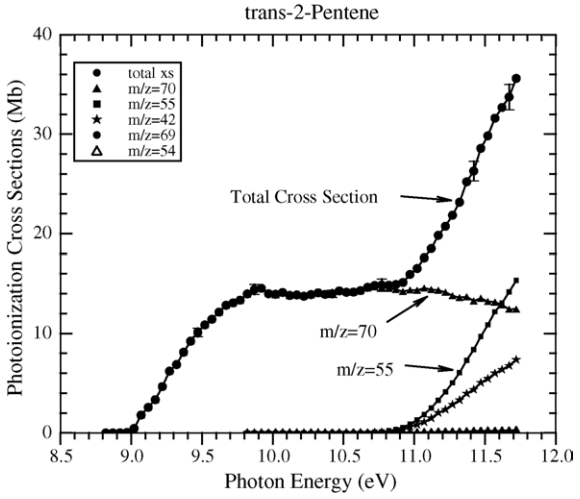

Fig. 14. Parent ion $C_5H_{10}^+$ ($m/z = 70$) and $C_4H_7^+$ ($m/z = 55$) fragment ion photoionization cross sections for *trans*-2-pentene.

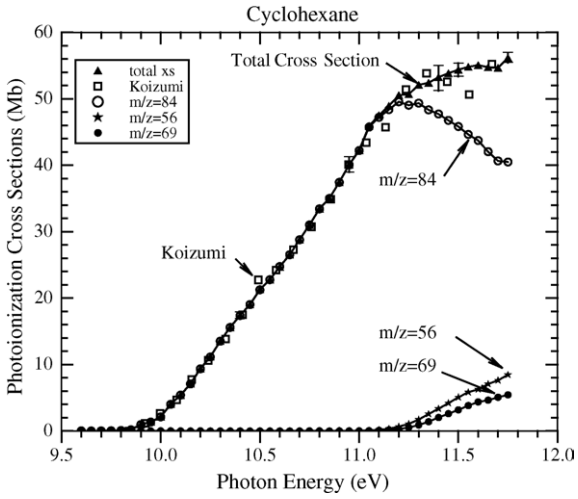

Fig. 16. Molecular and dissociative photoionization cross sections for cyclohexane. The total photoionization cross section is compared with the previous measurements of Koizumi et al. [46,61].

thresholds near 9 eV [5] to reach plateaus near 10 eV before dissociative ionization channels leading to $C_4H_7^+$ ($m/z = 55$) and $C_3H_6^+$ ($m/z = 42$) open near 10.7 eV [5]. The $C_3H_6^+$ cross sections required supplementary measurements of the fragmentation of *cis*- and *trans*-2-pentene in the absence of admixed propene. Traeger has recorded the photoionization efficiency for *cis*-2-pentene over this energy range [55], but no PIE data for *trans*-2-pentene have been reported.

The cyclopentene photoionization cross sections for parent $C_5H_8^+$ ($m/z = 68$) ions and $C_5H_7^+$ ($m/z = 67$) fragment ions are shown in Fig. 15. Here again the parent ion cross section rises from threshold near 9 eV [5] to a plateau near 10 eV before the onset of dissociative ionization near 11 eV [5]. The $C_5H_7^+$ fragment ion and total ionization cross sections rise steeply beyond the second ionization potential at 11.1 eV [43]. No previous cross section measurements for cyclopentene have been reported.

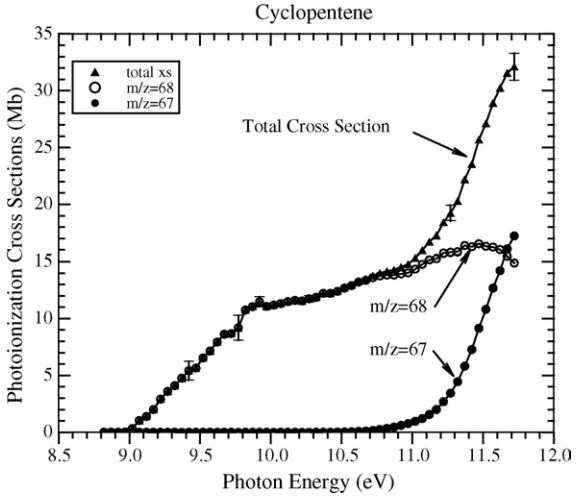

Fig. 15. Parent ion $C_5H_8^+$ ($m/z = 68$) and $C_5H_7^+$ ($m/z = 67$) fragment ion photoionization cross sections for cyclopentene.

3.7. Cyclohexane

Cyclohexane exhibits a parent ion cross section that increases gradually above threshold at 9.88 eV [5] in a fashion typical of other alkanes [56–58]. The fragment ions $C_3H_6^+$ ($m/z = 42$), $C_3H_7^+$ ($m/z = 43$), $C_4H_7^+$ ($m/z = 55$), $C_4H_8^+$ ($m/z = 56$), $C_5H_9^+$ ($m/z = 69$), and $C_6H_{11}^+$ ($m/z = 83$) have appearance potentials in the 11.1–11.5 eV range [5]. The most prominent fragment ions below 11.75 eV are $C_4H_8^+$ and $C_5H_9^+$, with cross sections shown in Fig. 16. Cross sections for $m/z = 42$, 43, and 55, not shown in Fig. 16, are given in the supplement to this paper. The $C_3H_6^+$ and $C_3H_7^+$ cross sections required supplementary measurements of the fragmentation of cyclohexane in the absence of admixed propene. The contribution of ^{13}C isotopomers of $C_3H_6^+$ is subtracted from the $C_3H_7^+$ ($m/z = 43$) ion signal. The $C_6H_{11}^+$ ion fragment reported by Sergeev et al. [59] was not observable at the detection limit of the present measurements. The parent photoionization cross section ($m/z = 84$) shown in Fig. 16 reaches a peak of 50 Mb near 11.2 eV before decreasing in competition with the dissociative ionization channels. The total ionization cross sections reported by Koizumi et al. [45,60] are in good agreement with the present measurements, as shown in Fig. 16.

3.8. Formic acid

The $HCOOH^+$ ($m/z = 46$) parent ion photoionization cross section of Fig. 17 exhibits a well-defined step for direct ionization to the $\upsilon_3' = 1$ state of the cation in agreement with previous studies of the photoelectron spectrum [61] and photoionization efficiency [62] of formic acid. The υ_3 mode is a C=O stretch with a frequency of 1495 cm^{-1} in the ground state of the cation [61]. The appearance energy for CHO_2^+ ($m/z = 45$) fragment ions at 12.3 eV [5,62] is nearly coincident with the second ionization potential at 12.38 eV [61]. The present measurements only extend to 12.41 eV, but the photoionization efficiency measurements of Villem et al. [62] indicate the $HCOOH^+$ parent

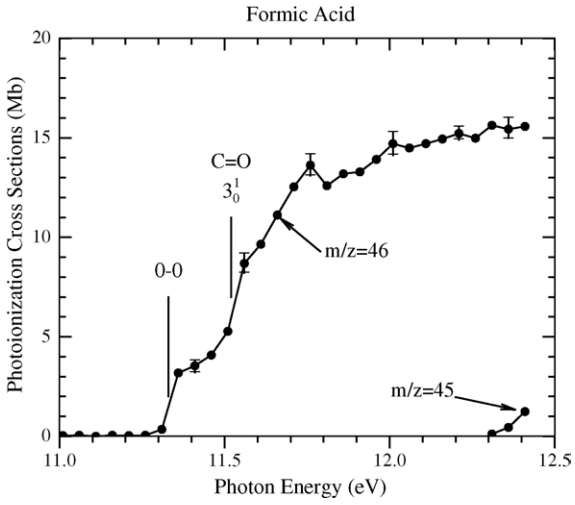

Fig. 17. Absolute cross sections for the photoionization of formic acid. A well-defined step for direct photoionization to the $v_3' = 1$ (C=O stretch) of the cation is indicated at 11.52 eV.

ion cross section remains nearly constant for photon energies to 13.5 eV.

4. Conclusion

The precision of the present measurements, with typical standard deviations of less than 10%, is primarily a measure of the reproducibility of sample preparations rather than uncertainties in ion signal measurements. Although discrepancies of 20% between measurements performed in different laboratories with similar techniques are common, the careful procedures used by Person and Nicole [15] ensure that the uncertainty in their absolute cross section measurements for propene, used here as a calibration standard, is unlikely to exceed 10%. Possible errors in the mass discrimination factors (cf. Fig. 1) may be as large as 10% for the heaviest masses because of uncertainties in the normalization of the data for benzene to that of Rennie et al. [26] (cf. Fig. 5). With consideration of these factors, we assign an uncertainty of 20% in the cross sections reported here.

The primary purpose of this study is to provide reliable photoionization cross sections for PIMS studies of flame chemistry. The focus of these measurements is on the near-threshold region within about 2 eV of the adiabatic ionization energies. Unambiguous concentration measurements of flame species require knowledge of near-threshold cross sections for parent and fragment ions to guide the selection of photon energies to minimize fragment ion interferences [12]. The energy resolution of this work corresponds to that used for flame studies. Direct comparisons of the measured cross section for vinylacetylene of Fig. 8 with photoionization efficiency measurements performed in flame environments is included as a supplement to this paper (see supplementary data). This supplement contains tabulated cross sections for the 16 molecules discussed here, presented along with figures and tabulated cross sections for acetylene, ethylene, and propyne. The development and testing of comprehensive kinetic models of combustion chemistry will require measurements of photoionization cross sections for many additional stable and radical intermediate species. The measurement of absolute photoionization cross sections for radical species presents difficult experimental challenges, although recent progress has been achieved with measurements for propargyl, vinyl, allyl, and 2-propenyl radicals [63,64].

Acknowledgements

This research was supported by the U.S. Department of Energy, Office of Basic Energy Sciences, Division of Chemical Sciences, Geosciences, and Biosciences, and by the U.S. Army Research Office, Chemical Sciences Division. Sandia is a multi-program laboratory operated by Sandia Corporation, a Lockheed Martin Company, for the National Nuclear Security Administration under contract DE-AC04-94-AL85000. The Advanced Light Source is supported by the Director, Office of Science, Office of Basic Energy Sciences, Materials Sciences Division, of the U.S. Department of Energy under Contract No. DE-AC02-05CH11231 at Lawrence Berkeley National Laboratory. We wish to thank Tina Kasper and Matthew Law for assistance with sample preparations.

Appendix A. Supplementary data

Supplementary data associated with this article may be found, in the online version, at doi:10.1016/j.ijms.2005.08.018.

References

[1] J.W. Gallagher, C.E. Brion, J.A.R. Samson, P.W. Langhoff, J. Phys. Chem. Ref. Data 17 (1988) 9.
[2] S.G. Lias, J.E. Bartmess, J.F. Liebman, J.L. Holmes, R.D. Levin, W.G. Mallard, J. Phys. Chem. Ref. Data 17 (Suppl. 1) (1988) 1.
[3] J. Berkowitz, Photoabsorption, Photoionization and Photoelectron Spectroscopy, Academic Press, New York, 1979.
[4] J. Berkowitz, Atomic and Molecular Photoabsorption, Absolute Total Cross Sections, Academic Press, New York, 2002.
[5] P.J. Linstrom, W.G. Mallard (Eds.), NIST Chemistry WebBook, NIST Standard Reference Database Number 69, National Institute of Standards and Technology, Gaithersburg, MD, 2003.
[6] G. Cooper, J.E. Anderson, C.E. Brion, Chem. Phys. 209 (1996) 61.
[7] D.A. Shaw, D.M.P. Holland, M.A. MacDonald, A. Hopkirk, M.A. Hayes, S.M. McSweeney, Chem. Phys. 163 (1992) 387.
[8] T.J. Xia, T.S. Chien, C.Y.R. Wu, D.L. Judge, J. Quant. Spectrosc. Radiat. Transfer 45 (1991) 77.
[9] H. Koizumi, T. Yoshimi, K. Shinsaka, M. Ukai, M. Morita, Y. Hatano, J. Chem. Phys. 82 (1985) 4856.
[10] K. Kameta, M. Ukai, R. Chiba, K. Nagano, N. Kouchi, Y. Hatano, K. Tanaka, J. Chem. Phys. 95 (1991) 1456.
[11] T.A. Cool, K. Nakajima, T.A. Mostefaoui, F. Qi, A. Mcllroy, P.R. Westmoreland, M.E. Law, L. Poisson, D.S. Peterka, M. Ahmed, J. Chem. Phys. 119 (2003) 8356.
[12] T.A. Cool, K. Nakajima, C.A. Taatjes, A. Mcllroy, P.R. Westmoreland, M.E. Law, A. Morel, Proc. Combust. Inst. 30 (2004) 1631.
[13] C.A. Taatjes, D.L. Osborn, T.A. Cool, K. Nakajima, Chem. Phys. Lett. 394 (2004) 19.
[14] C.A. Taatjes, S.J. Klippenstein, N. Hansen, J.A. Miller, T.A. Cool, J. Wang, M.E. Law, P.R. Westmoreland, Phys. Chem. Chem. Phys. 7 (2005) 806.
[15] J.C. Person, P.P. Nicole, Argonne National Laboratory Radiological Physics Division Annual Report, July 1967–June 1968, ANL 7489, p. 105.

[16] K. Watanabe, F.M. Matsunaga, H. Sakai, Appl. Opt. 6 (1967) 391.
[17] J.A.R. Samson, L. Yin, J. Opt. Soc. Am. B 6 (1989) 2326.
[18] J.A.R. Samson, J. Opt. Soc. Am. 54 (1964) 6.
[19] N. Wainfan, W.C. Walker, G.L. Weissler, J. Appl. Phys. 24 (1953) 1318.
[20] J.C. Person, J. Chem. Phys. 43 (1965) 2553.
[21] J.C. Person, P.P. Nicole, J. Chem. Phys. 49 (1968) 5421.
[22] J.C. Person, P.P. Nicole, J. Chem. Phys. 53 (1970) 1767.
[23] J.C. Person, P.P. Nicole, J. Chem. Phys. 55 (1971) 3390.
[24] J.C. Person, P.P. Nicole, Argonne National Laboratory Radiological Physics Division Annual Report, July 1969–June 1970, ANL 7760, p. 97.
[25] H. Koizumi, J. Chem. Phys. 95 (1991) 5846.
[26] E.E. Rennie, C.A.F. Johnson, J.E. Parker, D.M.P. Holland, D.A. Shaw, M.A. Hayes, Chem. Phys. 229 (1998) 107.
[27] K. Kameta, N. Kouchi, M. Ukai, Y. Hatano, J. Electron Spectrosc. Relat. Phenom. 123 (2002) 225.
[28] P.A. Heimann, M. Koike, C.W. Hsu, D. Blank, X.M. Yang, A.G. Suits, Y.T. Lee, M. Evans, C.Y. Ng, C. Flaim, H.A. Padmore, Rev. Sci. Instrum. 68 (1997) 1945.
[29] A.G. Suits, P. Heimann, X. Yang, M. Evans, C.W. Hsu, K.T. Lu, Y.T. Lee, A.H. Kung, Rev. Sci. Instrum. 66 (1995) 4841.
[30] W.C. Wiley, H.I. McLaren, Rev. Sci. Instrum. 26 (1955) 1150.
[31] A.J.C. Nicholson, J. Chem. Phys. 39 (1963) 954.
[32] J.B. Armitage, E.R.H. Jones, M.C. Whiting, J. Chem. Soc. 9 (1951) 44.
[33] H. Koizumi, T. Yoshimi, K. Hironaka, S. Arai, M. Ukai, M. Morita, H. Nakazawa, A. Kimura, Y. Hatano, Y. Ito, Y. Zhang, A. Yagashita, K. Ito, K. Tanaka, Radiat. Phys. Chem. 32 (1988) 111.
[34] D.M.P. Holland, D.A. Shaw, Chem. Phys. 243 (1999) 333.
[35] Y. lida, F. Carnovale, S. Davies, C.E. Brion, Chem. Phys. 105 (1986) 211.
[36] J.A.R. Samson, G.N. Haddad, T. Masuoka, P.N. Pareek, D.A.L. Kilcoyne, J. Chem. Phys. 90 (1989) 6925.
[37] J.A.R. Samson, W.C. Stolte, J. Electron Spectrosc. Relat. Phenom. 123 (2002) 265.
[38] E.L. Knuth, in: G.S. Springer, D.J. Patterson (Eds.), Engine Emissions: Pollutant Formation and Measurement, Plenum, New York, 1973, pp. 319–363.
[39] P.K. Sharma, E.L. Knuth, W.S. Young, J. Chem. Phys. 64 (1976) 4345.
[40] J.D. Bittner, Ph.D. Thesis, Massachusetts Institute of Technology, January 1981.
[41] K.M.A. Refaey, W.A. Chupka, J. Chem. Phys. 48 (1968) 5205.
[42] J.C. Person, P.P. Nicole, Argonne National Laboratory Radiological Physics Division Annual Report, July 1973–June 1974, ANL 75-3, p. 53.
[43] M.J.S. Dewar, S.D. Worley, J. Chem. Phys. 50 (1969) 654.
[44] H. Koizumi, K. Hironaka, K. Shinsaka, S. Arai, H. Nakazawa, A. Kimura, Y. Hatano, Y. Ito, Y. Zhang, A. Yagashita, K. Ito, K. Tanaka, J. Chem. Phys. 85 (1986) 4276.
[45] H. Koizumi, T. Yoshimi, K. Hironaka, S. Arai, M. Ukai, M. Morita, H. Nakazawa, A. Kimura, Y. Hatano, Y. Ito, Y. Zhang, A. Yagashita, K. Ito, K. Tanaka, Radiat. Phys. Chem. 32 (1988) 111.
[46] P. Bruckmann, M. Kessinger, J. Electron Spectrosc. Relat. Phenom. 2 (1973) 341.
[47] F. Brogli, E. Heilbronner, J. Wirz, E. Kloster-Jensen, R.G. Bergman, K.P.C. Vollhardt, A.J. Ashe III, Helv. Chim. Acta 58 (1975) 2620.
[48] W.L. Smith, Proc. R. Soc. A 300 (1967) 519.
[49] W.C. Price, A.D. Walsh, Trans. Faraday Soc. 41 (1945) 381.
[50] V.E. Bondybey, J.H. English, J. Chem. Phys. 71 (1979) 777.
[51] J.P. Maier, F. Thommen, J. Chem. Phys. 73 (1980) 5616.
[52] A.C. Parr, F.A. Elder, J. Chem. Phys. 49 (1968) 2659.
[53] R. Botter, J.M. Pechine, H.M. Rosenstock, Int. J. Mass Spectrom. Ion. Phys. 25 (1977) 7.
[54] J.J. Butler, D.M.P. Holland, A.C. Parr, R. Stockbauer, Int. J. Mass Spectrom. Ion. Processes 58 (1984) 1.
[55] J.C. Traeger, J. Phys. Chem. 90 (1986) 4114.
[56] R.I. Schoen, J. Chem. Phys. 37 (1962) 2032.
[57] W.A. Chupka, J. Berkowitz, J. Chem. Phys. 47 (1967) 2921.
[58] K. Kameta, N. Kouchi, M. Ukai, Y. Hatano, J. Electron Spectrosc. Relat. Phenom. 123 (2002) 225.
[59] Y.L. Sergeev, M.E. Akopyan, F.I. Vilesov, Y.V. Chizhov, High Energ. Chem. 7 (1973) 369.
[60] H. Koizumi, K. Shinsaka, Y. Hatano, Radiat. Phys. Chem. 34 (1989) 87.
[61] M. Schwell, S. Leach, K. Hottmann, H.-W. Jochims, H. Baumgartel, Chem. Phys. 272 (2001) 77.
[62] Y.Y. Villem, M.E. Akopyan, F.I. Vilesov, High Energ. Chem. 9 (1975) 356.
[63] J.C. Robinson, N.E. Sveum, D.M. Neumark, J. Chem. Phys. 119 (2003) 5311.
[64] J.C. Robinson, N.E. Sveum, D.M. Neumark, Chem. Phys. Lett. 383 (2004) 601.